

Measurement of π^0 v_2 in Au+Au Collisions at 200 GeV with the sPHENIX Detector

The sPHENIX Collaboration

Abstract

The sPHENIX detector and the Relativistic Heavy Ion Collider's 2023 commissioning dataset is used to measure the elliptic flow (v_2) of neutral pions (π^0 's) in 200 GeV Au+Au collisions via the scalar product method. π^0 candidates are reconstructed using the Electromagnetic Calorimeter, and the Minimum Bias Detector is used to determine the reference flow for the $v_2^{\pi^0}$ measurements. The $v_2^{\pi^0}$ values extracted from the scalar product method are consistent with previous PHENIX measurements. This analysis looks at π^0 candidates with $2 \leq p_T \leq 5$ GeV in 0–60% centrality events. These results validate the performance of the EMCal in the sPHENIX detector and demonstrate the potential of the physics mission of the sPHENIX experiment.

1 Introduction

By colliding heavy ions at high energies in accelerators like the Relativistic Heavy Ion Collider (RHIC) and the Large Hadron Collider (LHC), quark-gluon plasma (QGP), the primordial state of matter last seen microseconds after the Big Bang, can be created. Investigating QGP offers a unique opportunity to explore the transformation of energetic quarks and gluons into a strongly interacting state. This rapid formation of the QGP allows for an examination of its properties and the intricate, multi-scale quantum dynamics of its evolution [1]. A hallmark of QGP formation, and one of the most striking observations in heavy-ion collisions, is the collective motion of produced particles known as hydrodynamic flow [2]. This results from the hydrodynamic response of QGP to the geometric configuration and fluctuations of the initial state formed in the overlap region of the two colliding nuclei.

Anisotropic flow is characterized by a Fourier series where the magnitude of the Fourier coefficients (v_n) describe specific flow contributions. v_2 characterizes the elliptic flow contribution which is the extent of the ellipticity of the initial overlap region in collision events.

The sPHENIX experiment is a new collider detector at RHIC focused on jet and heavy-flavor probes of the QGP [3], which took commissioning data in 2023. This analysis is based on data from the sPHENIX commissioning run, taken in June and July 2023, and makes use of the combined information from the sPHENIX Electromagnetic Calorimeter (EMCal) and the Minimum Bias Detector (MBD) to measure the second-order flow coefficients (v_2) for π^0 's via the Scalar Product (SP) Method [4].

In this analysis, π^0 candidates are reconstructed and their invariant masses are computed via the diphoton decay channel in the EMCal. The resultant mass distribution is fit, and the v_2 is calculated for candidates within 2σ of the π^0 resonance peak. The MBD serves as the reference detector, with which π^0 candidate flow vectors are paired with event-wise flow vectors to compute the measured v_2 . Background subtraction is then performed, yielding the elliptic flow coefficient of the π^0 , $v_2^{\pi^0}$.

2 sPHENIX Detector

The sPHENIX experiment [5, 3] at RHIC provides coverage over full azimuth and pseudorapidity $|\eta| < 1$ around the collision point. The experiment consists of a variety of subsystems, including hadronic and electromagnetic calorimeters, a superconducting magnet, tracking subsystems, and a trigger system. This analysis uses data taken with the EMCal, a tungsten-scintillating fiber read-out with silicon photo-multipliers (SiPMs) coupled with light guides, and the MBD, which consists of a north and south arm, each containing 64 Cherenkov radiator PMTs.

The sPHENIX EMCal is used to measure photons to reconstruct π^0 's in this analysis. The EMCal has a large solid angle coverage of $|\eta| < 1.1$ and 2π in ϕ . During the 2023 commissioning run, subsystems were in partial operation, and the EMCal was read out in the region $-0.9 < \eta < 1.1$. The detector is comprised of 6144 blocks, each containing an array of 2×2 towers. Each block is made of a matrix of tungsten powder and epoxy with 2668 embedded scintillating fibers, and a readout that utilizes SiPMs. One block corresponds to approximately 0.05 radians in ϕ and 0.05

units of pseudorapidity in η . Blocks are organized into 64 sectors (32 azimuthal \times 2 longitudinal) and are projective in both η and ϕ , but pointing slightly off the collision axis in ϕ to minimize boundary effects between the blocks. Because of this projectivity, the length of the block varies, but is approximately $20X_0$, where $X_0 = 7\text{mm}$ is the radiation length. This slight non-projectivity also ensures that photons effectively interact with the absorber and form showers, thereby preventing channeling, in which photons could bypass the absorber if the blocks were aligned perfectly with the axis. From the Molière radius for the blocks, a cluster of 5×5 towers (or 2.5×2.5 blocks) contains over 95% of electromagnetic shower energy. In test-beam measurements, the EMCal has an energy resolution of $15.5\%/\sqrt{E} \oplus 2.9\%$ [6].

The MBD, covering the very forward region in $3.61 < |\eta| < 4.51$, is a reuse of the Beam-Beam Counter (BBC) from PHENIX due to the already extensive understanding of the BBC's operation, maintenance, cooling and calibration needs [5]. The MBD is comprised of 64 PMTs on each of the two arms, referred to as the North and South arms. The PMTs are arranged in 3 concentric rings around the beam-pipe, covering 2π in azimuth. The PMTs are arranged in a hexagonal formation with two small gaps in the PMT layout for the mounting structure. The MBD is used for minimum bias, centrality-selected event triggering, and samples approximately 90% of the inelastic hadronic cross-section in 200 GeV Au+Au collisions. [3]. The signal sum from both MBD arms is used to determine event centrality. Signals from the MBD PMTs are also used within this analysis to calculate flow vectors in collision events.

3 Data Selection

The analysis employs a combination of minimum bias (MB) and central triggered (Central) runs from the 2023 Au+Au data taking. The MB trigger requires that at least two PMTs fire in each section of the MBD. The central trigger is a modification of the MB trigger, requiring a higher count of PMTs to initiate an event. For the centrality ranges of 0–60% and 0–40% for the MB and Central event selection, respectively, the MBD based trigger is fully efficient.

Two types of cuts are imposed in the event selection process: the satisfaction of the minimum bias criteria and a vertex of $|z| < 10$ cm. The minimum bias classifier used in this analysis requires at least two PMTs fire on each MBD arm and an MBD charge of at least 10 in the North arm or at most 150 in the South. The z-vertex criteria, as determined by the MBD, ensures the events originate from z-vertices near zero, optimizing the kinematic coverage of the EMCal. These criteria select 1.78 million MB-triggered events and 2.45 million central-triggered events for this analysis.

4 Analysis

A tower-by-tower energy calibration is performed in rings of η using the data collected with the EMCal, over two steps. First, the energy response of the towers in a given η ring is balanced by fitting the slopes of the energy distributions for individual towers separately and scaling them to match each other, thus making the tower response uniform in ϕ . Clusters are formed from the grouping of contiguous EMCal towers together, with the splitting of clusters that have multiple local maxima. The clustering algorithm used is applied to the particular geometry of the sPHENIX

EMCal [5].

Pairs of clusters are then formed and the position of the π^0 peak was determined. η -dependent calibration constants which move the π^0 mass peak to the expected value are extracted based on the η location of the most energetic tower within the higher energy cluster of the pair. This procedure is done iteratively until the calibration is stable for all η rings. Monte Carlo simulations show that the expected value of the π^0 mass peak is higher than the nominal π^0 mass due to energy smearing within the calorimeter. The π^0 mass peak is higher than the expected value of 139.57 MeV due to the finite EMCal energy resolution, in agreement with observations in the data.

In reconstructing the π^0 candidates, each pair of clusters in the event that satisfies cuts of $\chi^2 < 4$ and $E_{\text{Core}} \geq 1$ GeV is considered. The cluster χ^2 is a measure of how likely the cluster has originated from a photon shower in the EMCal. This is derived from photon simulations of the detector in p+p collisions. The χ^2 reduces possible contamination from clusters originating from hadronic showers. The cluster core energy (E_{Core}) is a measurement provided by the EMCal's clustering algorithm that is designed to address the distortion in energy measurement caused by overlapping clusters in high-multiplicity events. This measurement extrapolates the core energy based on the central four or five towers within a cluster, following an electromagnetic shower profile developed and validated through beam tests [7]. The $E_{\text{Core}} \geq 1$ GeV requirement is applied to exclude clusters that originate from noise in the EMCal.

For each π^0 candidate, a cluster energy asymmetry of $\alpha < 0.5$ is required. This asymmetry is defined as:

$$\alpha \equiv \frac{|E_1 - E_2|}{E_1 + E_2}, \quad (1)$$

where E_1 and E_2 are the energies of the clusters of the π^0 candidate [7]. The cluster energy asymmetry discriminates against non- π^0 background pairs, exploiting the characteristic that the asymmetry distribution is approximately flat for true π^0 pairs, but skewed towards highly asymmetric pairs otherwise.

After applying the selection criteria, invariant mass ($M_{\gamma\gamma}$) distributions of π^0 candidates with $2 \leq p_T \leq 5$ GeV are generated for six centrality selections from 0–60%. The distributions are fit with a combined Gaussian and second-order polynomial function, in which the Gaussian fits the signal and the polynomial the combinatorial background. Figure 1 shows the invariant mass distributions for each analysis bin, where the vertical black lines mark the signal bounds, calculated in the range $\mu_{\text{Gauss}} \pm 2\sigma_{\text{Gauss}}$. Here, μ_{Gauss} denotes the Gaussian mean (peak position), and σ_{Gauss} the standard deviation (peak width). The fit is performed over the range $0.1 < M_{\gamma\gamma} < 0.35$ GeV, with the upper bound optimized to adequately cover the background while excluding the influence of the η meson (with $M_{\eta} = 0.55$ GeV), and the lower bound is set to exclude the region $M_{\gamma\gamma} < 0.1$ GeV, where the distribution sharply drops due to the effects of the cuts.

Based on these fits, the signal-to-background ratio (S/B) is calculated. A second-order polynomial function, initialized with coefficients from the combined fit, estimates the background by evaluating the center of each bin within the defined signal region. The signal is then estimated by subtracting this background from the total content of each bin.

Another crucial aspect of this analysis is the calculation of reference flow vectors (\vec{Q}_n) using the signals of individual MBD elements with the SP method, propagated to the v_2 calculation. \vec{Q}_n are

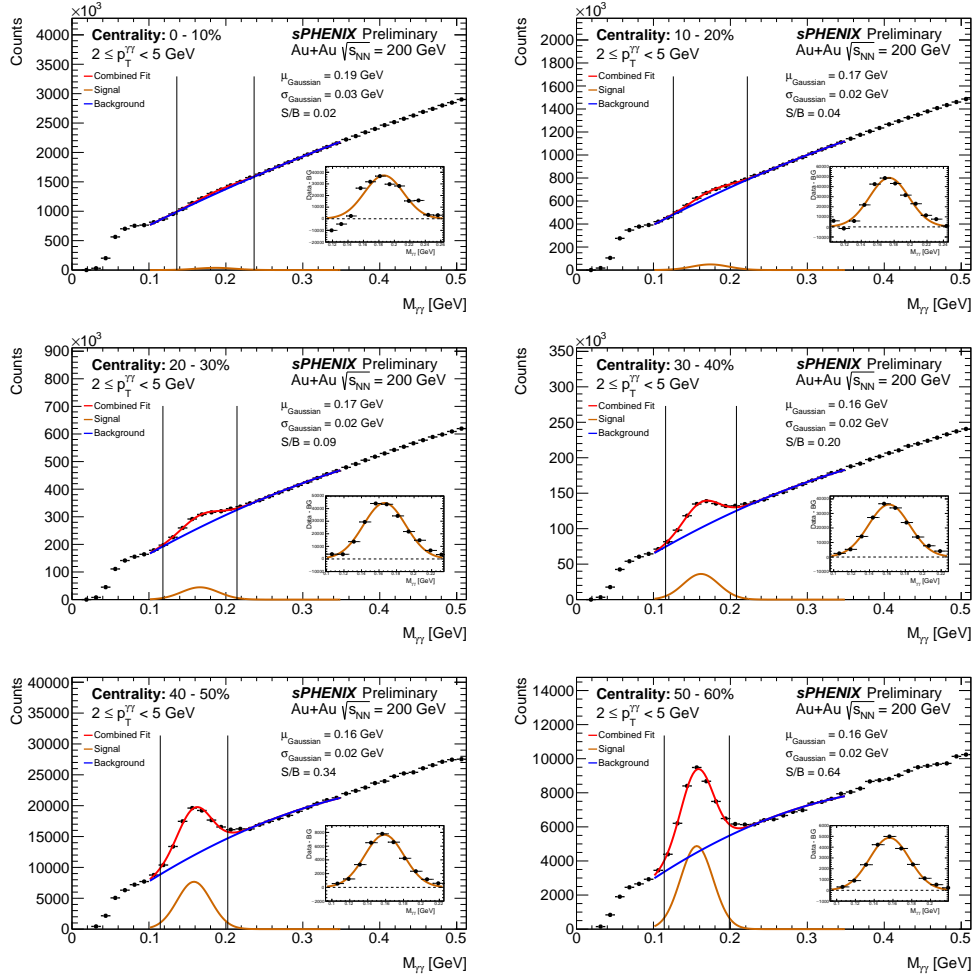


Figure 1: Invariant mass distributions for each centrality bin. The red curve is the total fit, the orange curve is the Gaussian used to fit the signal, and the blue curve is the polynomial used to fit the combinatorial background. The insets show the fitted mass peak after background subtraction. The uncertainties in these invariant mass distributions are statistical only.

calculated using information from the MBD with the SP Method defined as

$$v_n\{SP\} \equiv \text{Re} \frac{\langle \vec{q}_{n,j} \vec{Q}_n^S | N^* \rangle}{\sqrt{\langle \vec{Q}_n^S \vec{Q}_n^{N^*} \rangle}}. \quad (2)$$

Here,

$$\vec{q}_{n,j} = e^{in\phi_j} \quad (3)$$

is the n th-order q -vector of a given π^0 candidate in an event with azimuthal angle ϕ_j . Q_n is defined as:

$$\vec{Q}_n = \frac{1}{\sum_j \omega_j} \sum_j \omega_j \vec{q}_{n,j} \quad (4)$$

and is the reference flow vector in the event. \vec{Q}_n^N and \vec{Q}_n^S are measured using only PMTs in the North and South MBD arms respectively, and \vec{Q}_n is the result of summing over all MBD PMTs in Equation 4. The weighting factor, ω_j , is the PMT signal.

This asymmetry from the MBD mounting structure is accounted for in flow vectors found using the MBD in two steps. First, the average \vec{Q}_n is calculated over many events, and a recentering correction is applied to each event, based on the expectation that $\langle \vec{Q}_n \rangle = 0$ for an ideal detector. This correction is applied to each event as

$$\vec{Q}_{n, \text{recentered}} = \vec{Q}_{n, \text{raw}} - \langle \vec{Q}_{n, \text{raw}} \rangle \quad (5)$$

where $\langle \vec{Q}_{n, \text{raw}} \rangle$ is the uncorrected flow vector averaged over all events. A second flattening correction is then applied to the flow vectors to correct for persisting nonuniformities caused by detector irregularities, where the mean corrected \vec{Q}_2 is multiplied by the normalized inverse square root of the covariance matrix, given by

$$\frac{1}{\sqrt{N}} \begin{pmatrix} \langle Q_{2,y}^2 \rangle + D & -\langle Q_{2,x} Q_{2,y} \rangle \\ -\langle Q_{2,x} Q_{2,y} \rangle & \langle Q_{2,x}^2 \rangle + D \end{pmatrix} \quad (6)$$

where $D = \sqrt{\langle Q_{n,x}^2 \rangle \langle Q_{2,y}^2 \rangle - \langle Q_{2,x} Q_{2,y} \rangle^2}$ and $N = D(\langle Q_{2,x}^2 \rangle + \langle Q_{2,y}^2 \rangle + 2D)$ [8].

This flow vector is also related to the event plane angle, Ψ_n [9], where Ψ_n is the azimuthal angle of \vec{Q}_n , and is thus

$$\Psi_n = \frac{1}{n} \text{atan2} \left(\frac{Q_x}{Q_y} \right). \quad (7)$$

Although the event plane angle is not used explicitly in this analysis, Ψ_2 is used for quality assurance of \vec{Q}_2 . Over many events, the distribution of event plane angles is expected to be flat, since collision events have no bias toward flow in a certain direction relative to the detector. As shown in Figure 2, the recentering and flattening corrections to the flow vectors result in an overall flat distribution of event plane angles for the 20-30% centrality.

Background subtraction is done with an analytically derived procedure using the v_2 for real π^0 's ($v_2^{\pi^0}$), all diphoton pairs within the signal region of $\mu - 2\sigma < M_{\gamma\gamma} < \mu + 2\sigma$ (v_2^M), and background diphoton pairs outside the signal region in $\mu + 3\sigma < M_{\gamma\gamma} < 0.5$ GeV (v_2^{BG}). The relationship between the three is given by

$$v_2^{\pi^0} = v_2^M + \frac{v_2^M - v_2^{BG}}{S/B}. \quad (8)$$

To evaluate the statistical uncertainties on the nominal value of $v_2^{\pi^0}$, a sub-sampling procedure is used, where the total event pool is uniformly and randomly divided into 30 samples and the $v_2^{\pi^0}$ is measured for each sample via the SP method. The statistical uncertainty is calculated as the standard deviation of the obtained $v_2^{\pi^0}$ distribution divided by the square root of the effective number of samples. Statistical uncertainties are generally most significant in the central bin due to the large background, resulting in substantial v_2 variance from the subsampling procedure.

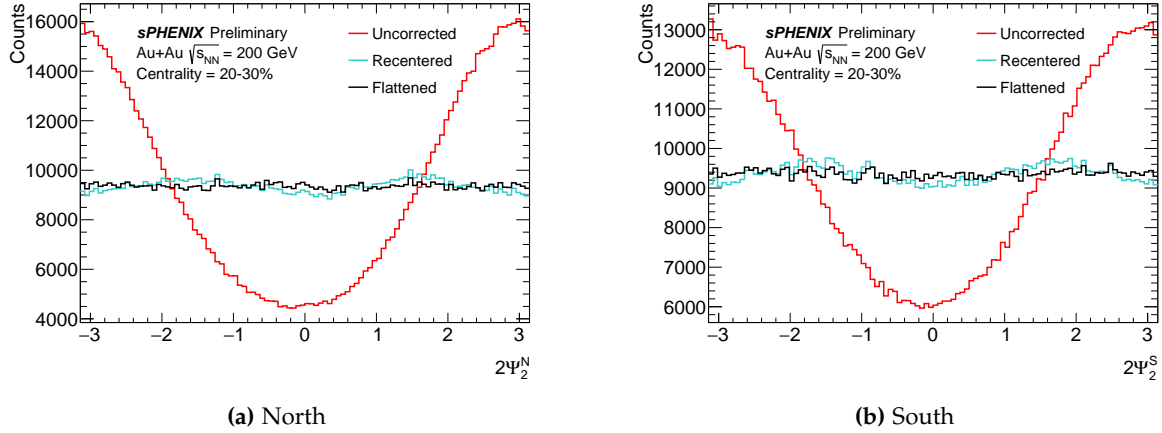


Figure 2: Event plane angles from the North (a) and South (b) arms of the MBD. Red shows the distribution of uncorrected Ψ_2 , and the blue and black lines show the distribution of Ψ_2 calculated with flow vectors that have been corrected with the recentering correction and both the recentering and flattening corrections, respectively.

5 Systematic Uncertainties

This measurement considers three primary sources of systematic uncertainties: variations in the signal window, background window, and different components of the EMCal energy scale calibration.

To assess the impact on $v_2^{\pi^0}$ from variations in the diphoton selection range, measured v_2 is computed within an alternative range of $\mu - 1.5\sigma < M_{\gamma\gamma} < \mu + 1.5\sigma$, in addition to the standard range $\mu - 2\sigma < M_{\gamma\gamma} < \mu + 2\sigma$. By tightening this region, the number of accepted diphotons is restricted, and subsequently, the S/B is increased. Similarly, to estimate the systematic uncertainty associated with variations in the background window selection, this window is adjusted from $\mu + 3\sigma < M_{\gamma\gamma} < 0.5 \text{ GeV}$ to $\mu + 3\sigma < M_{\gamma\gamma} < 0.4 \text{ GeV}$, and again the absolute differences from the reference v_2 is calculated.

Finally, to quantify the effects of uncertainties in the EMCal energy scale calibration, several sources of uncertainty were evaluated: statistical uncertainties in the π^0 -based calibration, the absolute scale uncertainty, and uncertainties based on the method used to balance the tower responses around ϕ . Each uncertainty is varied independently, and the analysis is repeated under that variation to assess the impact on the measured $v_2^{\pi^0}$. The systematic uncertainties on the $v_2^{\pi^0}$ values due to the EMCal energy scale, signal window, and background window range from 0.01 to 0.09, 0.001 to 0.04, and 0.002 to 0.03 respectively. Due to the evaluation procedure used to extract the various systematic uncertainties, the statistical precision can influence their estimated size particularly in the most statistics limited bins. Therefore the reported systematic uncertainties are a conservative choice, and additional statistics are expected to lead to a significant reduction in the systematic uncertainties.

6 Results

To summarize the results, $v_2^{\pi^0}$ is analyzed as a function of centrality. In Figure 3, the results for $v_2^{\pi^0}$ integrated over the range of $2 \leq p_T \leq 5$ GeV, are shown in six 10% wide centrality intervals from 0–60%. The results are overlaid with p_T -integrated data from a 2010 PHENIX measurement in Au+Au collisions at $\sqrt{s_{NN}} = 200$ GeV [10]. Good agreement is observed between the two measurements across the full centrality range studied. The PHENIX measurement is made with a significantly larger event sample, and thus this comparison serves as a useful verification, demonstrating that the trends observed in published $v_2^{\pi^0}$ results agree with this analysis. The results confirm the expected geometric dependence of the second-order azimuthal anisotropy, as measured in nucleus-nucleus collisions at RHIC and the LHC.

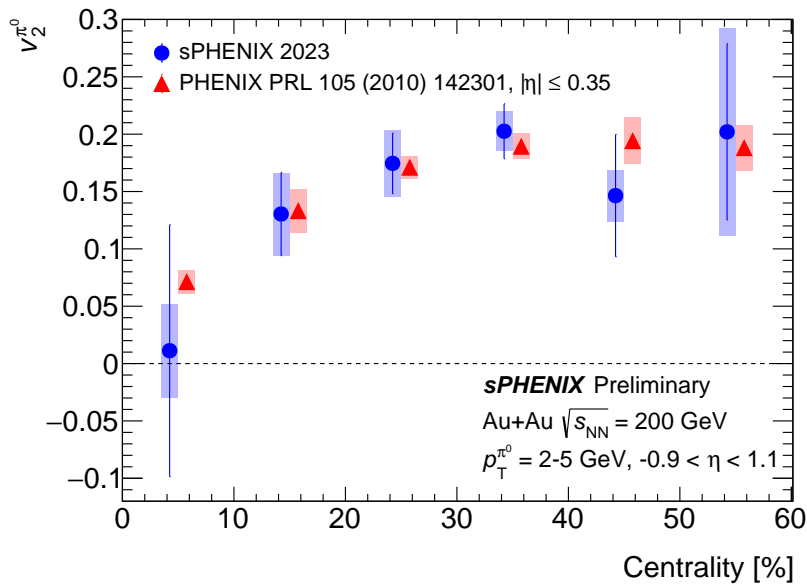


Figure 3: $v_2^{\pi^0}$ as a function of centrality, integrated over the range of $2 \leq p_T \leq 5$ GeV. The results, shown in blue with both statistical and systematic uncertainties, are offset to the left, while PHENIX data (p_T integrated), shown in red, is displaced to the right in each centrality bin for visibility.

7 Conclusion

Using the sPHENIX detector at RHIC, the $v_2^{\pi^0}$ is calculated from Au+Au collisions in bins of centrality, integrated over p_T , via an implementation of the Scalar Product method. Over the range of $2 \leq p_T \leq 5$ GeV and centrality 0–60%, the $v_2^{\pi^0}$ reconstructed in this analysis agrees with measurements taken in Au+Au events with the PHENIX detector via the reaction plane method. Using the partial dataset recorded during the commissioning process, this analysis observes signatures of QGP consistent with previous measurements at RHIC, confirming the performance of these important components of the sPHENIX experiment. This analysis is part of the first step in the sPHENIX data-taking program to answer fundamental open questions about the state and behavior of QGP, laying the foundation for future measurements leveraging the capabilities of the

sPHENIX EMCal to complete the scientific mission of both sPHENIX and RHIC.

References

- [1] Wit Busza, Krishna Rajagopal, and Wilke van der Schee. Heavy Ion Collisions: The Big Picture, and the Big Questions. *Ann. Rev. Nucl. Part. Sci.*, 68:339–376, 2018. [arXiv:1802.04801](https://arxiv.org/abs/1802.04801). 1
- [2] Björn Schenke. Flow in heavy-ion collisions—theory perspective. *Journal of Physics G: Nuclear and Particle Physics*, 38(12):124009, Nov 2011. [doi:10.1088/0954-3899/38/12/124009](https://doi.org/10.1088/0954-3899/38/12/124009). 1
- [3] sPHENIX Collaboration. sPHENIX Beam Use Proposal, 2022. URL: https://indico.bnl.gov/event/15845/attachments/40963/68517/sPHENIX_Beam_Use_Proposal_2022.pdf. 1, 2
- [4] C. Adler et al. Elliptic flow from two- and four- particle correlations in Au + Au collisions at $\sqrt{s_{NN}} = 130$ GeV. *Phys. Rev. C*, 66:034904, 2002. [arXiv:nuc1-ex/0206001](https://arxiv.org/abs/nuc1-ex/0206001). 1
- [5] sPHENIX Collaboration. sPHENIX Technical Design Report, 2019. URL: https://indico.bnl.gov/event/7081/attachments/25527/38284/sphenix_tdr_20190513.pdf. 2, 4
- [6] C. A. Aidala et al. Design and Beam Test Results for the 2-D Projective sPHENIX Electromagnetic Calorimeter Prototype. *IEEE Trans. Nucl. Sci.*, 68(2):173–181, 2021. [arXiv:2003.13685](https://arxiv.org/abs/2003.13685). 2
- [7] S. Afanasiev et al. High- p_T π^0 Production with Respect to the Reaction Plane in Au + Au Collisions at $\sqrt{s_{NN}} = 200$ GeV. *Phys. Rev. C*, 80:054907, 2009. [arXiv:0903.4886](https://arxiv.org/abs/0903.4886). 4, 4
- [8] Michael Clark. *Femtoscopic signatures of small QGP droplets in proton-lead collisions at the Large Hadron Collider*. PhD thesis, Columbia U., 2019. [doi:10.7916/d8-t50g-tn57](https://doi.org/10.7916/d8-t50g-tn57). 4
- [9] Matthew Luzum and Jean-Yves Ollitrault. Eliminating experimental bias in anisotropic-flow measurements of high-energy nuclear collisions. *Physical Review C*, 87(4), Apr 2013. [doi:10.1103/physrevc.87.044907](https://doi.org/10.1103/physrevc.87.044907). 4
- [10] A. Adare et al. Azimuthal Anisotropy of π^0 Production in Au + Au Collisions at $\sqrt{s_{NN}} = 200$ GeV: Path-Length Dependence of Jet Quenching and the Role of Initial Geometry. *Physical Review Letters*, 105(14), Sep 2010. [doi:10.1103/physrevlett.105.142301](https://doi.org/10.1103/physrevlett.105.142301). 6